Neurosci. Bull. August, 2019, 35(4):673–687
https://doi.org/10.1007/s12264-019-00353-0

www.neurosci.cn
www.springer.com/12264

ORIGINAL ARTICLE

Rac1 Modulates Excitatory Synaptic Transmission in Mouse Retinal Ganglion Cells

Ling-Zhu Li[1] · Ning Yin[1] · Xue-Yan Li[1] · Yanying Miao[1] · Shuo Cheng[1] · Fang Li[1] · Guo-Li Zhao[1] · Shu-Min Zhong[1] · Xin Wang[1] · Xiong-Li Yang[1] · Zhongfeng Wang[1]

Received: 26 August 2018 / Accepted: 21 October 2018 / Published online: 19 March 2019

Abstract Ras-related C3 botulinum toxin substrate 1 (Rac1), a member of the Rho GTPase family which plays important roles in dendritic spine morphology and plasticity, is a key regulator of cytoskeletal reorganization in dendrites and spines. Here, we investigated whether and how Rac1 modulates synaptic transmission in mouse retinal ganglion cells (RGCs) using selective conditional knockout of Rac1 (Rac1-cKO). Rac1-cKO significantly reduced the frequency of AMPA receptor-mediated miniature excitatory postsynaptic currents, while glycine/$GABA_A$ receptor-mediated miniature inhibitory postsynaptic currents were not affected. Although the total GluA1 protein level was increased in Rac1-cKO mice, its expression in the membrane component was unchanged. Rac1-cKO did not affect spine-like branch density in single dendrites, but significantly reduced the dendritic complexity, which resulted in a decrease in the total number of dendritic spine-like branches. These results suggest that Rac1 selectively affects excitatory synaptic transmission in RGCs by modulating dendritic complexity.

Keywords Rac1 · Retinal ganglion cell · Excitatory synaptic transmission · Dendrite · Dendritic spine

Electronic supplementary material The online version of this article (https://doi.org/10.1007/s12264-019-00353-0) contains supplementary material, which is available to authorized users.

✉ Zhongfeng Wang
zfwang@fudan.edu.cn

[1] Department of Neurology, Institutes of Brain Science, State Key Laboratory of Medical Neurobiology and MOE Frontiers Center for Brain Science, Zhongshan Hospital, Fudan University, Shanghai 200032, China

Introduction

Ras-related C3 botulinum toxin substrate 1 (Rac1), a member of the Rho GTPase family, is a low-molecular-weight guanine nucleotide-binding protein that functions as a binary switch by cycling between an active GTP-bound form and an inactive GDP-bound form [1, 2]. The activity of Rac1 is positively regulated by guanine nucleotide exchange factors (GEFs) and negatively regulated by GTPase-activated proteins [3, 4], and is inhibited by guanine nucleotide dissociation inhibitors [1, 5, 6]. Rac1 and its effector and regulatory proteins constitute a complex signaling network which regulates a variety of neuronal functions such as cytoskeletal dynamics, axon growth and guidance, cell survival, dendritic arborization, spine morphogenesis, excitatory synapse formation, and synaptic plasticity [1–3, 7–12].

Rac1 is widely expressed in mouse retinal cells including photoreceptors, horizontal cells, amacrine cells, retinal ganglion cells (RGCs), and Müller cells [13]. Increasing evidence has suggested that Rac1 is involved in retinal diseases. For example, overexpression of the dedicator of cytokinesis 3, a GEF for Rac1, prevents RGC degeneration in the glaucomatous retina by suppressing the glutamate neurotoxicity and oxidative stress mediated by N-methyl-D-aspartate receptor subunit NR2B [14]. Selective activation of distinct Rac1-dependent pathways improves RGC survival and prevents the degeneration of RGC dendrites in an optic nerve-crush mouse model [15]. In addition, activation of Rac1 induces reactive oxygen species production and then stimulates p65 nuclear factor-κB phosphorylation, thus increasing tumor necrosis factor-α release from retinal microglial cells [16]. Rac1 is activated in the streptozotocin-induced rat model of diabetes, and this may mediate diabetes-induced damage and/or alterations to the

blood-retinal barrier by increasing the vascular permeability of the retina [17].

RGCs, the only output neurons of the retina, integrate and process excitatory signals from bipolar cells and inhibitory signals from amacrine cells [18–21]. Any factors that affect the synaptic transmission of RGCs may modulate the processing of visual information. Although Rac1 has been shown to be involved in some retinal diseases, whether and how Rac1 modulates the synaptic transmission of RGCs is still largely unknown. In this study, by crossing Chat-cre mice with Rac1-floxed mice to obtain selective RGC conditional Rac1-knockout (Rac1-cKO) mice, we characterized the effects of Rac1 on the synaptic transmission of RGCs and the possible underlying mechanisms.

Materials and Methods

Animals

All experimental procedures were performed in accordance with the National Institutes of Health Guide for the Care and Use of Laboratory Animals and the Fudan University guidelines on the ethical use of animals, and were approved by the animal care committee of Institutes of Brain Science at Fudan University. C57BL/6 mice were obtained from SLAC Laboratory Animal Co., Ltd (Shanghai, China) and $Rac1^{flox/+}$ mice from The Jackson Laboratory (Bar Harbor, ME, USA). Tg(Chat-cre)GM24Gsat mice (Chat-$cre^{+/-}$) were a generous gift from Dr. Min-Min Luo at the National Institute of Biological Sciences (Beijing, China). All animals were housed under a 12-h light/dark cycle, with standard food and water provided *ad libitum*.

Generation and Gene Identification of Rac1-cKO Mice

Rac1-cKO mice were generated by crossing $Rac1^{flox/flox}$ mice with Chat-$cre^{+/-}$ mice. The genotypes of Chat-$cre^{+/-}$ mice, $Rac1^{flox/flox}$ mice, and Rac1-cKO mice were determined by polymerase chain reaction (PCR) using Premix Taq (TaKaRa, Japan) and the following primers: $Rac1^{flox/flox}$ forward, 5′-TCCAATCTGTGCTGCCCATC-3′, and $Rac1^{flox/flox}$ reverse, 5’ -GATGCTTCTAGGGGT-GAGCC-3′; Chat forward, 5′-GGTCTCCTTGTGGAG TGGGAGT-3′, and Chat reverse, 5′-CGGCAAACGG ACAGAAGCATT-3′. The Rac1 amplification protocol was as follows: 94°C/3 min (1 cycle); 94°C/30 s, followed by 65°C/1 min, followed by 72°C/1 min (35 cycles); and 72°C/2 min (1 cycle). The Cre^{+} amplification protocol was as follows: 94°C/5 min (1 cycle); 94°C/15 s, followed by 65°C/30 s, followed by 72°C/40 s (40 cycles); and 72°C/5 min (1 cycle). The PCR DNA products were then analyzed by 2% agarose gel electrophoresis.

Immunohistochemistry

Immunohistochemistry was performed as previously described [22, 23]. Briefly, each retina was vertically cut at 14 μm on a freezing microtome (Leica, Nussloch, Germany). The sections were blocked with 5% normal donkey serum and 1% bovine serum in phosphate-buffered saline (PBS) with 0.4% Triton X-100 at room temperature for 2 h. Then the sections were incubated with the following primary antibodies overnight at 4°C: monoclonal mouse anti-Rac1 (1:500 dilution; Abcam, Cambridge, MA, USA), monoclonal goat anti-Brn-3a (1:400; Santa Cruz Biotechnology, Santa Cruz, CA, USA), and polyclonal rabbit anti-Cre recombinase (1:1,000; Abcam). Binding sites of the primary antibodies were visualized by incubation with Cy3/Alexa Fluor 488/Alexa Fluor 647-conjugated donkey anti-rabbit, anti-mouse, or anti-goat IgG (1:400; Sigma-Aldrich, St. Louis, MO, USA) for 2 h at room temperature. The sections were photographed with a Leica SP2 confocal laser-scanning microscope. To avoid reconstruction stacking artifacts, double-labeled cells were precisely evaluated by sequential scanning on single-layer optical sections at intervals of 1.0 μm.

Hematoxylin and Eosin (H&E) Staining

H&E staining was performed as previously described [24]. Briefly, retinas embedded in paraffin were cut at 5 μm and stained with H&E (Sigma-Aldrich). The sections were photographed using an Olympus BX51 microscope under bright-field at 40× magnification.

Western Blot Analysis

Western blots were analyzed as we previously described [22, 23, 25]. Briefly, for whole-cell protein extraction, retinas were homogenized in RIPA lysis buffer supplemented with protease and phosphatase inhibitor cocktails (Roche Applied Science, Mannheim, Germany). For retinal plasma membrane protein extraction, we followed the protocol provided with the Plasma Membrane Protein Extraction Kit (BioVision, Milpitas, CA, USA). The concentration of total proteins was measured using a standard bicinchoninic acid assay kit (Pierce Biotechnology, Rockford, IL, USA). The extracted whole protein samples (1.0 μg/μL, 10 μL) and membrane protein samples (1.0 μg/μL, 20 μL) were resolved on 8%, 10%, and 15% SDS-PAGE according to the molecular weight of the target proteins using the Mini-Protean 3 Electrophoresis System (Bio-Rad, Hercules, CA), and then electroblotted onto

polyvinylidene fluoride membranes (Immobilon-P, Millipore, Danvers, MA, USA) using the Mini Trans-Blot Electrophoretic Transfer System (Bio-Rad, Hercules, CA, USA). After blocking in 5% non-fat milk at room temperature for 2 h, the membranes were incubated overnight at 4°C with the following primary antibodies: polyclonal mouse anti-GluN1 (1:1000; BD Pharmingen, Franklin Lakes, NJ), polyclonal rabbit anti-GluN2A (1:200; Alomone Labs, Jerusalem, Israel), polyclonal rabbit anti-GluN2B (1:200; Alomone Labs), polyclonal rabbit anti-GluA1 (1:200; Alomone Labs), monoclonal rabbit anti-mGluR1 (1:1000; Cell Signaling Technology, Danvers, MA), monoclonal rabbit anti-mGluR5 (1:500; Abcam), polyclonal rabbit anti-glycine receptor alpha1+alpha2 (1:1000; Abcam), and polyclonal rabbit anti-$GABA_A$ receptor alpha1 (GABRA1) (1:1000; Abcam). After washing in Tris-buffered saline-Tween 20, the membranes were incubated with horseradish-peroxidase-conjugated donkey anti-mouse or donkey anti-rabbit IgG (1:5000; Jackson Jackson Immuno-Research Laboratories, Wes Grove, PA) for 1 h at room temperature. The blots were then incubated with enhanced chemiluminescent reagent (ThermoFisher Scientific, Rockford, IL) and imaged with a digital imager (FluorChem E System, ProteinSimple, San Jose, CA). For sequential immunoblotting, the blots were washed with Tris-buffered saline, stripped with Restore Western Blot Stripping Buffer (ThermoFisher Scientific, Rockford, IL), and re-blocked and incubated with primary antibodies if necessary.

Retinal Slice Preparation

Retinal slices were made following our previously-described procedure [22, 26, 27]. Briefly, after deep anesthesia and euthanasia, the retinas were carefully removed and embedded in low-melting-point agarose (4% in artificial cerebral spinal fluid [ACSF]). Slices (200 μm) were cut on a vibratome (Leica, VT1000s, Nussloch, Germany) and transferred to a holding chamber where they were completely submerged in ACSF containing (in mmol/L) 125 NaCl, 2.5 KCl, 25 $NaHCO_3$, 1.25 NaH_2PO_4, 2.5 $CaCl_2$, 1 $MgCl_2$, and 10 glucose (pH 7.4), bubbled continuously with 95% O_2 and 5% CO_2, and maintained at room temperature (21°C–23°C) for at least 30 min before recording.

Preparation of Isolated RGCs

Retinal neurons were dissociated using enzymatic and mechanical methods as previously described [28, 29] with minor modifications. Briefly, the retinas were incubated in oxygenated Hank's solution containing (in mmol/L) 137 NaCl, 0.5 $NaHCO_3$, 1 NaH_2PO_4, 3 KCl, 2 $CaCl_2$, 1 $MgSO_4$, 20 HEPES, 16 glucose, 1 sodium pyruvate, pH 7.4 adjusted with CsOH, 310 mOsm/L, and then digested in Hank's solution containing 1.6 U/mL papain (Calbiochem, San Diego, CA, USA), and supplemented with 0.2 mg/mL L-cysteine for 30 min at 35°C. Fire-polished Pasteur pipettes were used to mechanically dissociate retinal neurons.

Electrophysiological Recordings

Whole-cell voltage-clamp recordings were made as described in our previous studies [22, 27, 29]. All experiments were done at room temperature. Patch pipettes were made by pulling BF150-86-10 glass (Sutter Instrument Co., Novato, CA) on a P-97 Flaming/Brown micropipette puller (Sutter Instrument Co.), then fire-polishing (Model MF-830, Narishige, Tokyo, Japan). Whole-cell membrane currents were recorded from RGCs using a patch amplifier (Axopatch700B; Molecular Devices, San Jose, CA) with a Digidata 1440A data acquisition board and pClamp 10.2 software (Molecular Devices). Fast capacitance was fully cancelled and cell capacitance was cancelled as much as possible by the amplifier circuits. Seventy percent of the series resistance of the recording electrode was compensated. Analog signals were sampled at 10 kHz, filtered at 1 kHz and stored for further analyses. The access resistance was monitored during recordings and if the change in resistance was ≥20%, the cell was discarded. Only one cell was recorded in each retinal slice.

For recordings, individual slices were transferred to a chamber that was continuously superfused with oxygenated ACSF at 1 mL/min–2 mL/min. RGCs were identified by their location and morphology with the assistance of infrared-differential interference contrast video microscopy (BX51WI, Olympus, Tokyo, Japan), and were further identified by intracellular injection of Alexa Fluor 488. To record evoked excitatory postsynaptic currents (eEPSCs), test stimuli were delivered at 0.05 Hz through a patch pipette filled with ACSF placed on the inner nuclear layer (INL) or inner plexiform layer (IPL), locations corresponding to the dendritic fields of the recorded RGCs. RGCs were voltage-clamped at –70 mV to +40 mV (adjusted liquid junction potential). α-Amino-3-hydroxy-5-methyl-4-isoxazolepropionic acid receptor (AMPAR)-mediated current amplitudes were measured as the maximum current at –70 mV, and *N*-methyl-D-aspartic acid receptor (NMDAR)-mediated current amplitudes were measured at 50 ms after the peak amplitude at +40 mV. The resistance of recording electrodes was typically 4 MΩ–8 MΩ after filling with the internal solution. To record miniature EPSCs (mEPSCs) and eEPSCs, the internal solution consisted of (in mmol/L): 120 $CsMeSO_3$, 5 NaCl, 2

EGTA, 10 HEPES, 2 ATP-Mg, 0.2 GTP-Na, 10 tetraethylammonium chloride (TEA-Cl), 3 QX-314, 5 Alexa Fluor 488, pH 7.2 adjusted with CsOH, 280–290 mOsm/L. To record miniature inhibitory postsynaptic currents (mIPSCs), the internal solution consisted of (in mmol/L): 150 CsCl, 0.1 $CaCl_2$, 1 EGTA, 10 HEPES, 4 ATP-Mg, 0.4 GTP-Na, 1 $MgCl_2$, 5 Alexa Fluor 488, pH 7.2 adjusted with CsOH, 280–290 mOsm/L.

For recordings in dissociated RGCs, the cells were superfused continuously with extracellular solution containing (in mmol/L): 115 NaCl, 2.5 KCl, 10 $BaCl_2$, 5 CsCl, 15 HEPES, 15 TEA-Cl, 10 glucose, and 0.5 μmol/L tetrodotoxin (TTX) adjusted to pH 7.4 with NaOH and osmolality to 300–310 mOsm/L with sucrose. Patch pipettes had resistance of 3-6 MΩ when filled with the following internal solutions. For whole-cell AMPA currents, the internal solution consisted of (in mmol/L) 120 $CsMeSO_3$, 5 NaCl, 2 EGTA, 10 HEPES, 2 ATP-Mg, 0.2 GTP-Na, 10 TEA-Cl, and QX-314 3, pH 7.2 adjusted with CsOH, 280–290 mOsm/L. For glycine currents, the internal solution consisted of (in mmol/L) 150 CsCl, 0.1 $CaCl_2$, 1 $MgCl_2$, 10 HEPES, 1 EGTA, 0.4 GTP-Na, 4 ATP-Mg, pH 7.2 adjusted with CsOH, 280–290 mOsm/L.

CN04 Administration

From postnatal day 8 (P8) onwards, Rac1-cKO mice received intraperitoneal injections of 20 μL of 5 μg/mL CN04 (Cytoskeleton Inc., Denver, CO, USA), an activator of Rho family GTPases, once daily until P17. CN04 was dissolved in 0.9% saline, and Rac1-cKO mice receiving injections of an equal volume of 0.9% saline served as controls.

Dendritic Morphological Analyses

The dendrite and dendritic spine-like branch densities of RGCs were analyzed in whole flat-mounted retinas. The retinas were mounted with the ganglion cell layer (GCL) upturned and RGCs were chosen using an infrared-differential interference contrast video microscope (BX51WI, Olympus). Lucifer Yellow (Sigma-Aldrich) was injected into cells as previously reported [30], with modifications. Briefly, a micropipette filled with a saturated solution of Lucifer Yellow was inserted into the soma of a selected RGC. Current pulses (3.3 Hz, 200 ms duration, 5 μA) were delivered for at least 3 min to facilitate dye entry into the cell. Three to five RGCs were injected in a single retina. After the injections, the retina was incubated overnight in 4% paraformaldehyde in PBS (pH 7.4), and then incubated with polyclonal rabbit anti-Lucifer Yellow (1:1000 dilution, ThermoFisher Scientific) at 4°C for 2 days. Binding sites of the primary antibody were visualized by incubation with Alexa Fluor 488-conjugated donkey anti-rabbit IgG (1:400; Sigma-Aldrich) at 4°C overnight. Z-stack images of RGCs were acquired using an FV1000 confocal laser scanning microscope with a 40× objective (Olympus) at intervals of 1 μm to capture dendritic images and with a 100× oil-immersion objective to capture dendritic spine-like branch images [31, 32]. The images were analyzed with a FluoView laser scanning confocal microscope (Olympus), Imaris software (Bitplane, Zurich, Switzerland), and Xuv Stitch software (Bitplane).

Statistical Analysis

mEPSC, mIPSC, and eEPSC data are represented as the median and range (maximum, minimum), while the other data are expressed as the mean ± SEM. Western blot data were analyzed using GraphPad Prism software (version 5.0; GraphPad Software, La Jolla, CA). Images of RGCs were analyzed using Imaris software (Bitplane). Electrophysiological data were analyzed using Mini-Analysis (Synaptosoft, Leonia, NJ), SigmaPlot (version 10.0, Systat Software Inc., San Jose, CA), and Igor 4.0 (WaveMetrics, Tigard, OR).

Comparisons between two groups used Student's *t*-test, and multiple comparisons were made using one-way analysis of variance and Bonferroni's *post hoc* test. Before using the *t*-test or one-way analysis of variance, the data were analyzed using the Kolmogorov-Smirnov test or Brown-Forsythe test to evaluate the normality or homogeneity of variance [33]. $P < 0.05$ was considered significant. In electrophysiological experiments, unless otherwise stated, "*n*" represents the number of RGCs. Only one cell was recorded in each retinal slice or Petri dish, and only one or two slices or Petri dishes obtained from the same mouse were used for recordings. In the other experiments, "*n*" represents the number of mice used in each group.

Results

Rac1 Modulates Synaptic Transmission in RGCs

Genotype screening by PCR showed a single 242-bp band in Rac1-cKO mice, while wild-type $Rac1^{+/+}$ mice showed a 115-bp band (Fig. S1A). The results of genotype screening of Chat-$cre^{+/-}$ mice are shown in Fig. S1B. The Rac1 protein expression levels in whole retinal extracts from Rac1-cKO mice were assessed using Western blot and were found to be significantly reduced to 76.8% ± 5.5% of the C57BL/6 controls ($n = 6$, $P = 0.002$) (Fig. S1C, D). We further investigated whether Rac1-cKO mainly occurs in RGCs. Choline acetyltransferase (ChAT), a rate-

limiting enzyme in the process of acetylcholine synthesis, is a definitive marker for cholinergic neurons [34]. However, it has been reported that in ChAT-cre/Gsat mice, the Cre recombinase is ectopically expressed in the GCL and the INL, where RGCs and their dendrites are localized [35]. In vertical retinal slices, Chat-cre recombinase was predominantly expressed in Brn-3a (brain-specific homeobox/POU domain protein 3A)-positive RGCs and the IPL (Fig. S1E). Double immunofluorescence labeling showed that Rac1 was abundantly expressed in the GCL and the IPL, and double-labeled with Brn-3a in control mice (Fig. S1F, f1–f4). Together, these results indicated that Rac1 expression in RGCs and the IPL was lower in Rac1-cKO mice (Fig. S1F, f5–f8), suggesting that Rac1 expression was primarily reduced in the RGCs.

We examined the effect of Rac knockout on retinal morphology using H&E staining of vertical sections and found no significant difference in morphology among the control, Rca1-cKO, and Chat-cre$^{+/-}$ mice in both the nasal and temporal retina (Fig. S1G). These results suggested that conditional deletion of Rac1 in RGCs has no significant influence on retinal structure.

Since the electrophysiological recordings were done from P17 to P21, we determined whether the endogenous Rac1 was already eliminated in RGCs at P17 using immunofluorescence triple-labeling. As shown in Fig. 1A, Rac1 was no longer detectable in the Brns-3a-positive RGCs expressing Cre recombinase, suggesting that the endogenous Rac1 is already lost at P17.

We then determined whether conditional deletion of Rac1 affects synaptic transmission in RGCs. First, mEPSCs were recorded in vertical retinal slices, with inhibitory $GABA_A$ and glycine receptors blocked by bicuculline (10 μmol/L) and strychnine (10 μmol/L), respectively. In addition, the fast Na^+ channel blocker tetrodotoxin (TTX; 500 nmol/L) was added to the perfusion solution to block action potential-mediated synaptic activity. Under these conditions, perfusion with ACSF containing the non-NMDAR antagonist CNQX (10 μmol/L) completely eliminated the mEPSCs, suggesting that mEPSCs are mediated by non-NMDARs (data not shown). Recordings in control and Rac1-cKO retinas showed that the frequency of mEPSCs in an RGC was significantly lower in the Rac1-cKO retina (Fig. 1B). On average, the median mEPSC frequency of RGCs in Rac1-cKO mice was 3.16 Hz (15.06 Hz, 1.34 Hz; n = 10, P = 0.002), significantly lower than the control value of 16.35 Hz (28.95 Hz, 3.68 Hz; n = 11) (Fig. 1C). However, conditional deletion of Rac1 in RGCs did not significantly change the amplitude of mEPSCs, the median being 9.75 pA (13.75 pA, 6.69 pA; n =10, P = 0.630), comparable to the control value of 8.50 pA (15.13 pA, 4.52 pA; n = 11) (Fig. 1D). Moreover, conditional deletion of Rac1 in RGCs had no effect on the kinetics of mEPSCs [rise-time, 2.60 ms (3.18 ms, 1.40 ms) (Rac1-cKO) *vs* 2.47 ms (3.30 ms, 1.58 ms) (control), P = 0.953; decay time, 9.80 ms (12.31 ms, 4.70 ms) (Rac1-cKO) *vs* 9.85 ms (18.85 ms, 5.54 ms) (control), P = 0.446] (Fig. 1E, F).

To test whether the above changes of mEPSCs in the RGCs of Rac1-cKO mice can be rescued by activating pathways parallel to Rac1, we gave CN04, an activator of Rho family GTPases, to Rac1-cKO mice. Intraperitoneal CN04 administration significantly rescued the decreased frequency of mEPSCs, with a median frequency of 7.71 Hz (15.42 Hz, 8.12 Hz; n = 13, P = 0.033 *vs* untreated Rac1-cKO mice). But the frequency was still lower than that of control wild-type mice (P = 0.021) (Fig. 1B, C). In addition, CN04 slightly increased the amplitude of mEPSCs, with a median of 12.48 pA (18.69 pA, 8.12 pA; n = 13, P = 0.031 *vs* untreated Rac1-cKO mice) (Fig. 1D). However, CN04 did not significantly change the kinetics of mEPSCs [rise-time, 2.40 ms (3.68 ms, 1.61 ms), P = 0.972 *vs* control and P = 0.970 *vs* untreated Rac1-cKO mice; decay time, 7.10 ms (12.97 ms, 5.16 ms), P = 0.054 *vs* control and P = 0.192 *vs* untreated Rac1-cKO mice] (Fig. 1E, F).

The reduction in the frequency of mEPSCs in Rac1-cKO mice suggested that either the presynaptic glutamate release probability is changed or postsynaptic mechanisms is involved. Since the conditional deletion of Rac1 principally occurred in RGCs, we speculated that postsynaptic mechanisms were involved. To test this, we recorded eEPSCs at holding potentials of +40 and −70 mV in RGCs in retinal slices from control and Rac1-cKO mice (Fig. 1G). The ratio of NMDA/AMPA current amplitude (+40 mV/−70 mV) was higher [0.99 (2.54, 0.04; n = 8, P = 0.013)] in Rac1-cKO RGCs than in controls [0.22 (0.93, 0.08; n = 9) (Fig. 1H). Furthermore, we compared the AMPAR-mediated currents in RGCs acutely isolated from control and Rac1-cKO mice. In these RGCs, most processes were destroyed during the isolation process, so the currents were mainly mediated by AMPARs in the somata. Current recordings in RGCs from control and Rac1-cKO mice (Fig. 1I) showed no significant difference in the amplitude induced by 100 μmol/L AMPA, with a mean current density of 24.1 ± 5.1 pA/pF (n = 10) for control mice and 25.6 ± 3.5 pA/pF (n = 9, P = 0.813) for Rac1-cKO mice (Fig. 1J). These results suggested that conditional deletion of Rac1 in RGCs does not change AMPARs in the somata of RGCs.

We then examined the effect of conditional deletion of Rac1 on glycine receptor-mediated mIPSCs in RGCs by blocking excitatory receptors with CNQX (10 μmol/L) and D-APV (50 μmol/L), and blocking $GABA_A$ receptors with bicuculline (10 μmol/L). In addition, the fast Na^+ channel blocker TTX (500 nmol/L) was added to the perfusion

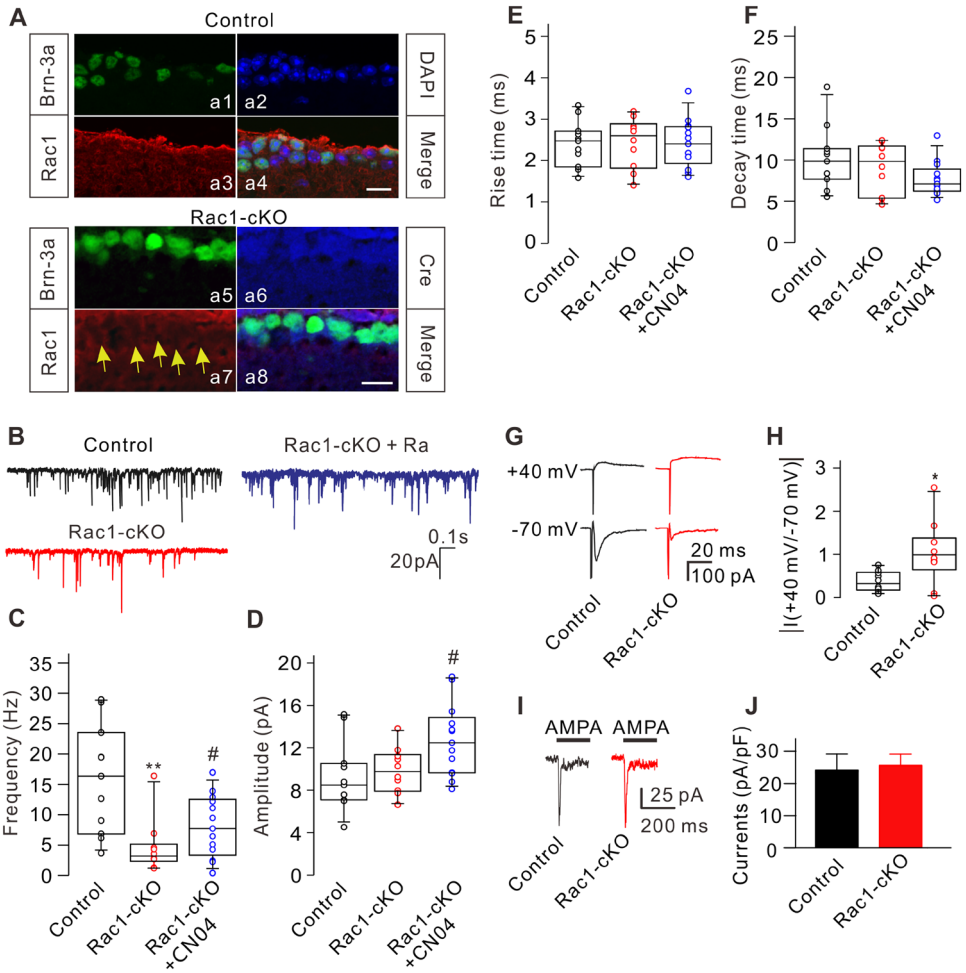

Fig. 1 Conditional knockout of Rac1 modulates excitatory synaptic transmission of RGCs. **A** Triple immunofluorescence labeling showing the expression of Brn-3a (**a1**), DAPI (**a2**), and Rac1 (**a3**) in a retinal slice from a control mouse at P17 (**a4**: merged image of **a1**, **a2**, and **a3**). Triple immunofluorescence labeling showing the expression of Brn-3a (**a5**), Cre recombinase (**a6**), and Rac1 (**a7**) in a retinal slice from an Rac1-cKO mouse at P17 (**a8**: merged image of **a5**, **a6**, and **a7**). Arrows indicate RGCs lacking Rac1 expression. Scale bars, 10 μm. **B** Representative recordings of mEPSCs in RGCs from control, Rac1-cKO, and Rac1-cKO+CN04 retinal slices. **C–F** Summary data showing that conditional deletion of Rac1 in RGCs reduced the frequency (**C**), but not the amplitude (**D**) and kinetics (**E, F**) of mEPSCs. CN04 administration partially rescued the decreased frequency of mEPSCs in RGCs from Rac1-cKO mice (n = 11-13; $^{**}P < 0.01$ *vs* control, $^{\#}P < 0.05$ *vs* Rac1-cKO). **G** Representative recordings showing the changes in amplitude of eEPSCs from RGCs in retinal slices at holding potentials of +40 mV and –70 mV in control and Rac1-cKO mice. **H** Summary data showing the average ratios of the current amplitudes at +40 mV and –70 mV in RGCs from control (n = 9) and Rac1-cKO (n = 8) mice ($^{*}P < 0.05$ *vs* control). **I** Representative recordings from two RGCs acutely isolated from control and Rac1-cKO mice, showing no significant difference in the currents induced by AMPA (100 μmol/L). **J** Summary data showing the average AMPA current densities in RGCs acutely isolated from control (n = 10) and Rac1-cKO (n = 9) mice. The distribution of data in each cell was indicated as scattered circles and the data are expressed as medians and interquartile ranges.

solution to block action potential-mediated synaptic activity. Conditional deletion of Rac1 in RGCs had no significant effect on glycine receptor-mediated mIPSCs (Fig. 2A). On average, the median frequency [0.12 Hz (4.64 Hz, 0.04 Hz), n = 12, P = 0.164] and amplitude [16.38 pA (55.23 pA, 5.85 pA), n = 12, P = 0.680] in Rac1-cKO mice did not differ from controls [frequency, 0.85 Hz (8.15 Hz, 0.03 Hz), n = 10; amplitude, 21.94 pA (53.70 pA, 17.18 pA), n = 10] (Fig. 2B, C). Conditional deletion of Rac1 also did not change the kinetics of glycine receptors, with a median rise time of 4.05 ms (5.37 ms, 3.08 ms; n = 12, P = 0.081) and decay time of 26.80 ms (44.06 ms, 10.11 ms; n = 12, P = 0.852), both of which were similar to the control [rise time, 3.17 ms (6.88 ms, 2.36 ms), n = 10; decay time, 20.20 ms (32.38 ms, 11.96 ms), n = 10] (Fig. 2D, E). Similarly, conditional deletion of Rac1 had no significant effect on $GABA_A$ receptor-mediated mIPSCs (Fig. 2F). When we recorded $GABA_A$ receptor-mediated mIPSCs, excitatory synaptic transmission was blocked by CNQX (10 μmol/L) and D-APV (50 μmol/L), and glycine

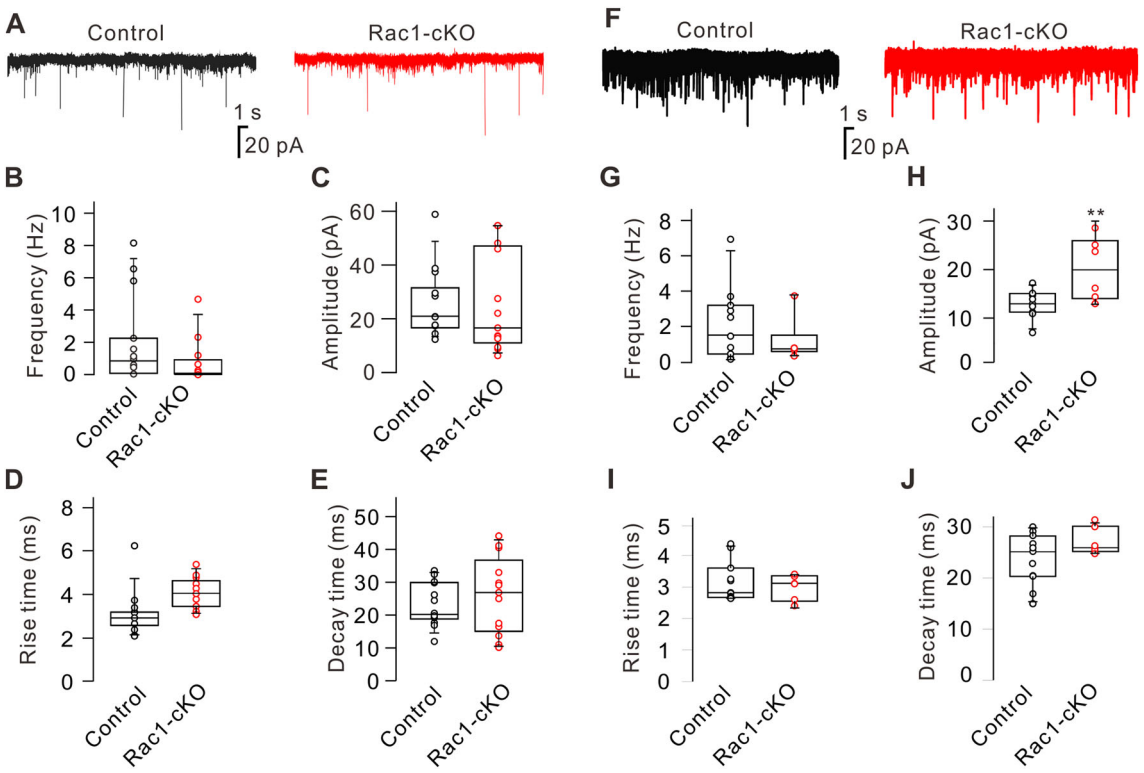

Fig. 2 Conditional knockout of Rac1 does not affect glycine and $GABA_A$ receptor-mediated inhibitory synaptic transmission in RGCs. **A** Representative recordings of glycine receptor-mediated mIPSCs in RGCs from control and Rac1-cKO retinal slices. **B–E** Summary data showing the frequency (**B**), amplitude (**C**), rise-time (**D**), and decay time (**E**) of mIPSCs in RGCs from control (n = 12) and Rac1-cKO (n = 10) mice. **F** Representative recordings of $GABA_A$ receptor-mediated mIPSCs in RGCs from control and Rac1-cKO retinal slices. **G–J** Summary data showing the frequency (**G**), amplitude (**H**), rise time (**I**), and decay time (**J**) of $GABA_A$-receptor-mediated mIPSCs in RGCs from control (n = 11) and Rac1-cKO (n = 6) mice. $^{**}P < 0.01$ *vs* control. The distribution of data in each cell was indicated as scattered circles and the data are expressed as medians and interquartile ranges.

receptors were blocked by strychnine (10 μmol/L). TTX (500 nmol/L) was also applied to block fast Na^+ channels. The median frequency in Rac1-cKO mice [0.77 Hz (3.76 Hz, 0.35 Hz), n = 6, P = 0.280] was comparable to the control [1.60 Hz (7.33 Hz, 0.11 Hz), n = 11] (Fig. 2G). Although the median amplitude in RGCs from Rac1-cKO mice [20.56 pA (29.53 pA, 13.31 pA), n = 6, P = 0.005] was higher than the control value [13.28 pA (17.73 pA, 7.07 pA; n = 11)] (Fig. 2H), the median rise time [3.12 ms (3.41 ms, 2.41 ms; n = 6, P = 0.550)] and decay time [25.89 ms (31.07 ms, 24.62 ms; n = 6, P = 0.140)] did not significantly differ from those in controls [rise time, 2.82 ms (4.32 ms, 2.64 ms), n = 11; decay time, 25.10 ms (29.96 ms, 14.95 ms), n = 11] (Fig. 2I, J). These results suggested that conditional deletion of Rac1 in RGCs had no significant influence on the inhibitory synaptic transmission of RGCs.

Expression of Excitatory and Inhibitory Synaptic Receptor Subunits in RGCs of Rac1-cKO Mice

We then determined whether there are differences in synaptic receptor expression between Rac1-cKO mice and control mice at P70. Expression of the GluA1 subunit of AMPARs was higher in Rac1-cKO mice (Fig. 3A), the average protein level being 135.9% ± 14.9% of control (n = 6, P = 0.042) (Fig. 3B), while the protein level of the GluA2 subunit was unchanged (95.3% ± 4.0% of control; n = 6, P = 0.284) (Fig. 3C, D). Because conditional deletion of Rac1 caused a decrease in mEPSC frequency (Fig. 1B), and mEPSCs are mediated by AMPARs, the higher expression of GluA1 may not involve functional AMPARs. To test this possibility, we assessed the levels of the cytoplasmic (c-GluA1) and membrane (m-GluA1) components using Western blot analysis. The c-GluA1 level (206.1% ± 3.5% of control, n = 6, P = 0.031), but not the m-GluA1 level (100.2% ± 13.3% of the control, n = 6, P = 0.991), was significantly higher in Rac1-cKO mice than in controls, suggesting that functional AMPARs do

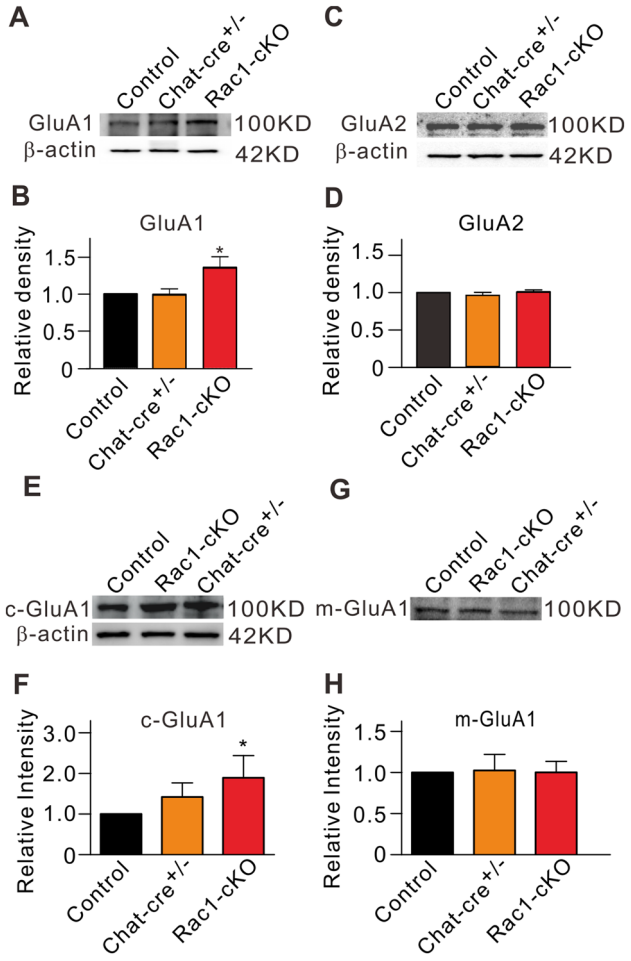

Fig. 3 Protein levels of GluA1 and GluA2 subunits of AMPARs in retinal extracts from Rac1-cKO, Chat-cre$^{+/-}$, and control mice. **A, C** Representative immunoblots of GluA1 (**A**) and GluA2 (**C**) protein levels. **B, D** Cumulative data showing the average densitometry of immunoreactive bands of GluA1 (**B**), GluA2 (**D**) expression. **E, G** Representative immunoblots showing the GluA1 protein levels of the cytoplasmic component (c-GluA1) (**E**) and membrane component (m-GluA1) (**G**). **F, H** Cumulative data showing the average densitometry of immunoreactive bands of c-GluA1 (**F**) and m-GluA1 (**H**) protein levels. All data are normalized to control. n = 6 for all groups. $^{*}P < 0.05$ *vs* control.

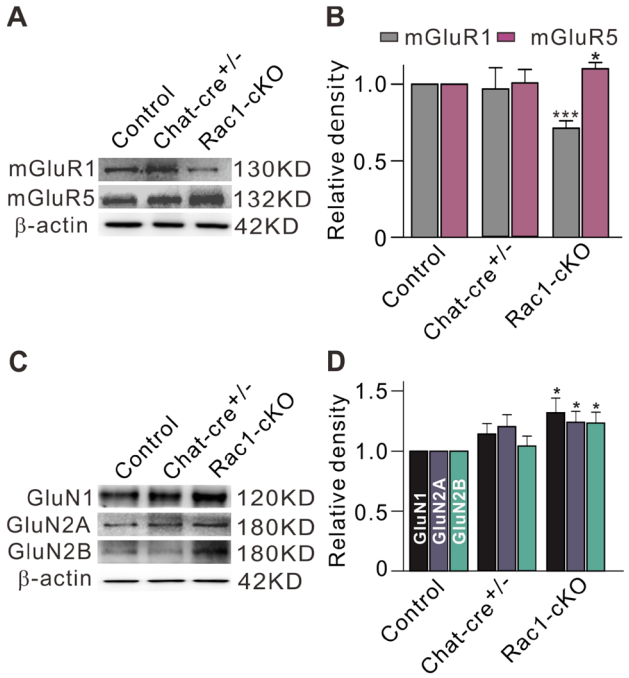

Fig. 4 Protein levels of mGluR1/5 and NMDAR subunits in retinal extracts from Rac1-cKO, Chat-cre$^{+/-}$, and control mice. **A** Representative immunoblots showing the mGluR1 and mGluR5 protein levels. **B** Bar charts summarizing the average densitometry of immunoreactive bands of mGluR1 and mGluR5 expression. **C** Representative immunoblots showing the GluN1, GluN2A, and GluN2B protein levels. **D** Bar charts summarizing the average densitometry of immunoreactive bands of GluN1, GluN2A, and GluN2B expression. All the data are normalized to control. n = 6–7. $^{*}P < 0.05$, $^{***}P < 0.001$ *vs* control.

not increase due to conditional deletion of Rac1 (Fig. 3E–H).

In addition, we determined the expression of mGluR Group I (mGluR I), including mGluR1 and mGluR5, by Western blot analysis. The mGluR1 protein level in Rac1-cKO retinas was significantly lower (71.3% ± 4.8% of control, n = 6, $P < 0.001$), while the mGluR5 protein level was significantly higher (110.2% ± 4.1% of control, n = 6, P = 0.032) (Fig. 4A, B).

We also assessed the expression levels of the GluN1, GluN2A, and GluN2B subunits of NMDARs. Conditional deletion of Rac1 induced an increase in the expression levels of all three subunits (Fig. 4C), the average protein levels increasing to 132.0% ± 12.2% (n = 6, P = 0.033), 124.1% ± 8.9% (n = 7, P = 0.020), and 123.4% ± 9.0% of control levels (n = 7, P = 0.022), respectively (Fig. 4D).

Consistent with the electrophysiological results, the expression levels of the inhibitory synaptic $GABA_A$, and glycine receptors were not significantly different (Fig. 5A, C). The protein levels of GABRA1 and glycine receptors in Rac1-cKO retinas were 127.2% ± 22.7% (n = 6, P = 0.249) and 105.7% ± 9.2% of control (n = 8, P = 0.541), respectively (Fig. 5B, D).

Having shown that the frequency of mEPSCs and expression of GluA1 were changed in Rac1-cKO retinas in mice at P17–P21 and P70, respectively, we determined whether the expression of GluA1 changed developmentally from postnatal week 2 (2W) to month 3 (3M). As shown in Fig. 6A, the GluA1 protein levels in both control and Rac1-cKO retinas from 1M to 3M did not differ from that at 2W. On average, the protein levels at 1M, 2M, and 3M in Rac1-cKO retinas were 108.5% ± 7.4% (n = 6, $P > 0.05$), 95.9% ± 9.9% (n = 6, $P > 0.05$), and 105.2% ± 8.5% of that at 2W (n = 6, $P > 0.05$), respectively (Fig. 6B),

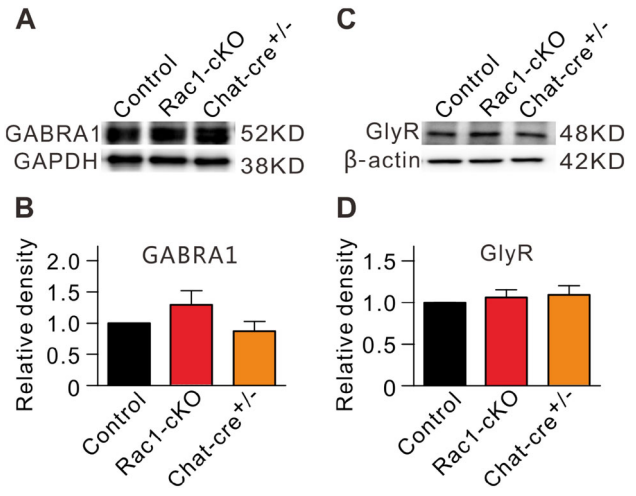

Fig. 5 No change in GABRA1 and glycine receptor protein levels in Rac1-cKO retinas. **A, C** Representative immunoblots showing the GABRA1 (**A**) and glycine receptor (GlyR) (**C**) expression in control, Rac1-cKO, and Chat-cre$^{+/-}$ retinal extracts. **B, D** Bar charts summarizing the average densitometry of immunoreactive bands of GABRA1 (**B**) and GlyR (**D**) expression in control, Rac1-cKO, and Chat-cre$^{+/-}$ retinal extracts. All the data are normalized to control. n = 6–8.

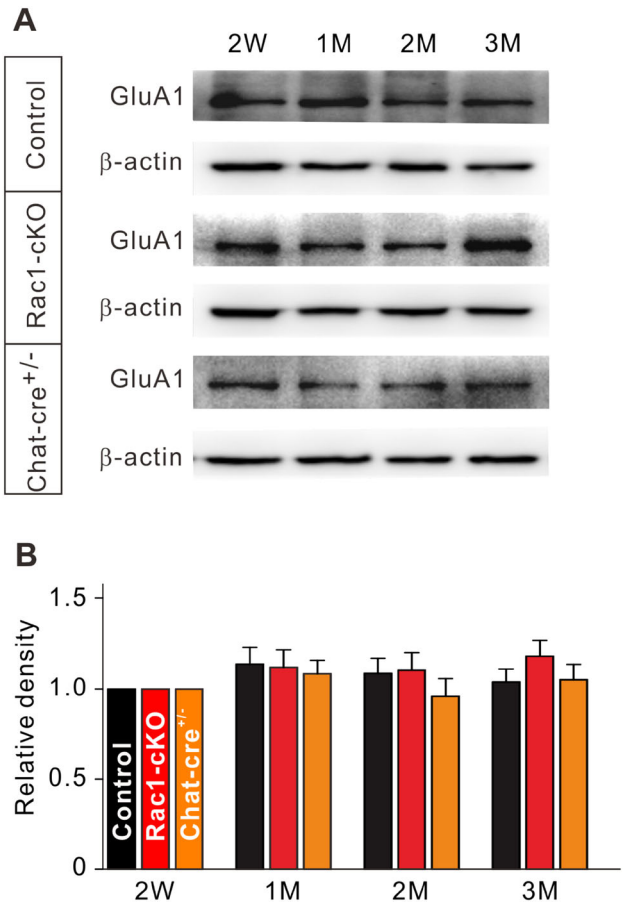

Fig. 6 Protein levels of GluA1 in extracts from Rac1-cKO, Chat-cre$^{+/-}$, and control retinas during the postnatal period from 2 weeks (2W) to 3 months (3M). **A** Representative immunoblots showing the GluA1 protein levels at different postnatal times (2W, 1M, 2M, 3M). **B** Bar charts summarizing the average densitometry of immunoreactive bands of GluA1 expression at different postnatal times. All the data are normalized to 2W. n = 6 for all groups.

suggesting that the development of GluA1 protein in RGCs was completed by 2W.

Rac1 Modulates the Dendritic Integrity of RGCs

Previous studies have demonstrated that Rac1 plays an important role in modulating the morphology of dendrites and spines [36–42]. Having shown that the frequency of mEPSCs was reduced in RGCs from Rac1-cKO mice, we used intracellular injection of Lucifer Yellow to determine whether Rac1 conditional knockout alters their dendrites and dendritic spine-like branches. RGCs were identified by the presence of an axon projecting to the optic disc. Any cells lacking an axon, even though they might possess the dendritic characteristics of typical RGCs, were not included in the analyses [32]. In total, 21 RGCs from 15 control mice (P17–P21) were randomly chosen for the analyses; these included all subtypes of RGCs (Table 1) in the classification by Sun *et al.* [43]. As the dendritic morphology of RGCs may have been altered by Rac1 conditional knockout, the 23 RGCs from 11 Rac1-cKO mice (P17–P21) were not identified by subtype. Representative RGC images from control and Rac1-cKO mice are shown in Fig. 7A. The dendritic field area of each dendrite was calculated by multiplying its length by its average width. Total dendritic field area (TDFA) was the sum of all dendrites measured. Rac1 conditional knockout significantly reduced the TDFA to 10,155 ± 1,509 μm^2 (n = 23, P = 0.019) from the control value of 14,714 ± 1,036 μm^2 (n = 21) (Fig. 7B). In addition, the total dendritic length of

Table 1 Percentages of different types of RGCs for dendritic analysis in retinas from C57BL/6 mice (n = 21).

RG_A	RG_B	RG_C	RG_D	Unclassified
4/21(19%)	6/21(28.6%)	9/21(42.9%)	1/21(4.8%)	1/21(4.8%)

RGCs from Rac1-cKO mice was also decreased to 2,195 ± 240 μm (n = 23, P = 0.007) from the control value of 3,065 ± 186 μm (n = 21) (Fig. 7C). To provide a physiological measure, we analyzed the differences in membrane capacitance using capacitance compensation during mEPSC recordings from RGCs in Rac1-cKO and control mice. Conditional deletion of Rac1 indeed induced a decrease in the membrane capacitance of RGCs (control, 34.2 ± 3.2 pF, n = 15; Rac1-cKO, 25.2 ± 2.7 pF, n = 12, P = 0.049).

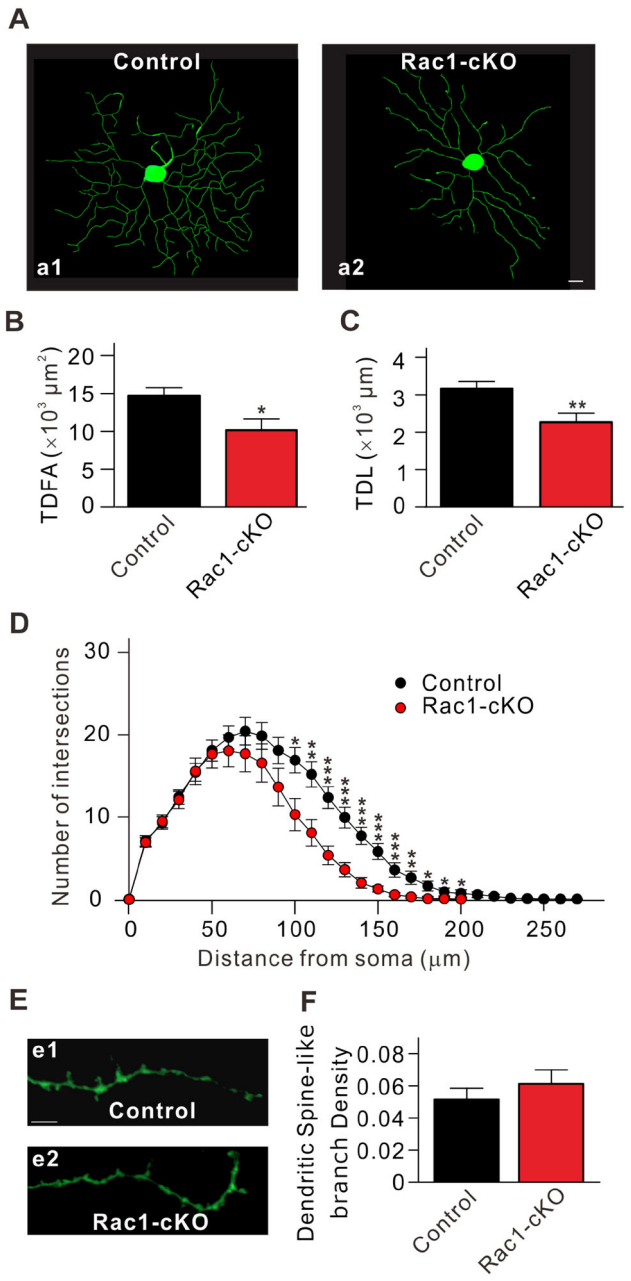

Fig. 7 Conditional deletion of Rac1 in RGCs reduces dendritic integrity. **A** Representative images of RGCs stained by Lucifer Yellow from control (**a1**) and Rac1-cKO mice (**a2**). Scale bar, 10 μm. **B, C** Quantitation of total dendritic field area (TDFA) (**B**) and total dendritic length (TDL) (**C**) of RGCs in control and Rac1-cKO mice (n = 21 for control and 23 for Rac1-cKO groups). **D** Sholl analysis of dendritic integrity of RGCs in control and Rac1-cKO mice (n = 21 for control and 23 for Rac1-cKO groups). **E** Representative images of dendritic spine-like branches of RGCs in control (**e1**) and Rac1-cKO (**e2**) mice. Scale bar, 10 μm. **F** Dendritic spine-like branch density of RGCs in control and Rac1-cKO mice (n = 21 for control and 38 for Rac1-cKO groups). *P < 0.05, **P < 0.01, ***P < 0.001 *vs* control.

We then analyzed the dendritic changes using Sholl analysis, which is widely used to quantify and graphically represent the characteristic morphology of dendritic arbors [44–50]. This analysis involved counting the numbers of intersections of dendrites with rings of increasing radii, in increments of 10 μm, centered on the soma of an RGC. The Sholl profile was obtained by plotting the number of intersections *versus* the radial distance from the soma [46, 51]. The dendritic complexity in Rac1-cKO mice was reduced at 50 μm from the soma (average number of intersections, 17.7 ± 1.7 (n = 23, P = 0.84), and a significant reduction was observed at 100 μm (control, 16.9 ± 1.5, n = 21; Rac1-cKO, 10.3 ± 2.0, n = 23; P = 0.012) to 200 μm (control, 0.71 ± 0.44, n = 21; Rac1-cKO, 0.04 ± 0.04, n = 23; P = 0.12) compared to the control (Fig. 7D). We further determined differences in the density of dendritic spine-like branches of RGCs in Rac1-cKO mice. In each cell, two secondary dendrites with a length ≥40 μm and two tertiary dendrites were chosen, and the total number of spine-like branches was counted (Fig. 7E). The average number of dendritic spine-like branches in 38 RGCs from Rac1-cKO mice was 0.06 ± 0.008/μm, similar to that in control mice (0.05 ± 0.007/μm, n = 21, P = 0.463) (Fig. 7F). These results suggested that even though the density of dendritic spine-like branches did not change, the total number of dendritic spine-like branches was lower in Rac1-cKO mice because of the reduced dendritic complexity of RGCs.

Discussion

Rac1 Selectively Modulates Excitatory Synaptic Transmission in RGCs

The Cre-LoxP recombination system is a powerful *in vivo* tool for gene deletion, overexpression, and ectopic expression in cells and tissues [52, 53]. Previous studies have reported that in ChAT-cre/Gsat mice, ChAT-Cre recombinase is ectopically expressed in RGCs, but not in cholinergic amacrine cells [35]. By crossing ChAT-cre/Gsat mice with $Rac1^{flox/flox}$ mice, we obtained Rac1-cKO mice and found that Rac1 knockout predominantly occurred in RGCs, and this was supported by Western blot and immunohistochemical analysis (Fig. S1). It should be noted that Rac1-cKO did not significantly influence retinal structure (Fig. S1G). This is different from some retinal diseases such as glaucoma in which the retinal IPL decreases in thickness due to RGC death [54]. We speculated that a partial decrease in the dendritic integrity of RGCs was not enough to change the thickness of the IPL since the reduced complexity of the dendritic tree was observed at 100–200 μm from the RGC soma (Fig. 7).

A major finding of this study was that conditional knockout of Rac1 selectively reduced excitatory synaptic transmission in RGCs, and this was supported by the

following findings. First, in Rac1-cKO mice, the frequency of mEPSCs was significantly decreased, but the amplitude and kinetics were not affected, suggesting that Rac1 knockout does not change the function of AMPARs and/or kainate receptors. In addition, it should be noted that CN04 administration partially rescued the decrease in mEPSC frequency and slightly increased the amplitude of mEPSCs (Fig. 2). This may have resulted from the activation of RhoA and Cdc42, because CN04 is not a specific Rac1 activator [55, 56]. Furthermore, it is possible that CN04 also increased the activity of presynaptic neurons which have an intact Rac1 pathway. Second, in Rac1-cKO mice, the ratio of NMDA/AMPA current amplitudes was increased (Fig. 2G, H), but the amplitudes of AMPAR-mediated currents recorded in the somata of dissociated RGCs were unchanged (Fig. 1I, J), suggesting that the changes in APMARs occur at postsynaptic sites, but not in the somata. Third, conditional knockout of Rac1 had no significant effect on mIPSCs (Fig. 2A–J), and in acutely isolated RGCs from Rac1-cKO mice, the glycine-induced current densities were similar to those of control mice (Fig. 2K, L).

Rac1 Modulates the Dendritic Integrity of RGCs

The mEPSCs recorded in RGCs are mediated by AMPARs [27]. Conditional deletion of Rac1 in RGCs reduced the frequency of mEPSCs, suggesting that the presynaptic glutamate release probability and/or postsynaptic mechanisms are involved. Based on the finding that in Rac1-cKO mice, conditional deletion of Rac1 predominantly occurred in RGCs, it is possible that retrograde signaling initiated by postsynaptic molecules eventually modulated presynaptic properties. Indeed, in a previous study [27], we found that endocannabinoid (eCB) released from RGCs retrogradely regulates neurotransmitter release from presynaptic neurons by activating CB1 receptors. To the best of our knowledge, eCB is the only known retrograde signal in the inner retina, although we cannot exclude other molecules. However, the synthesis and release of eCB requires strong depolarization of RGCs, and eCB modulates both excitatory and inhibitory synaptic transmission in RGCs [27]. In the present study, we found that Rac1-cKO only affected excitatory synaptic transmission. Therefore, we speculated that eCB may not be involved in the Rac1-cKO induced changes. Nevertheless, we plan to explore whether other retrograde molecules may be involved in future studies. On the other hand, postsynaptic mechanisms may be involved. However, Western blot analysis showed that the total GluA1 protein level was increased in Rac1-cKO mice (Fig. 3). Even though we demonstrated that the increased expression of GluA1 was in the cytoplasmic component (c-GluA1), the m-GluA1 level was still comparable to control mice, indicating that the total number of functional AMPARs in the membrane was not reduced. We found that the dendritic field and length of RGCs were reduced in Rac1-cKO mice, indicating a decrease in dendritic complexity, which resulted in a reduction in the total number of dendritic spine-like branches, thus contributing to the reduced mEPSC frequency. It should be noted that conditional deletion of Rac1 did not change the levels of m-GluA1. We speculate that the change in m-GluA1 levels in RGCs may have been undetectable because the protein sample was obtained from whole retinal homogenates. Indeed, the changes in protein expression in the whole extract cannot directly reflect changes in RGCs. It would be better to isolate pure RGCs, and then run Western blots. However, the synaptic receptors are expressed on the dendrites; it is difficult to obtain a complete RGC, including its soma and dendrites, from the retina. In the present study, Rac1 deletion mainly occurred in RGCs. Therefore, we speculate that the changes in synaptic receptor protein expression largely reflected changes in RGCs. Furthermore, our results showed that the c-GluA1 level in Rac1-cKO mice was significantly increased. Based on the fact that Rac1 is one of the major regulators of the actin cytoskeleton, we speculate that Rac1-cKO may affect the trafficking of GluA1, thus resulting in its accumulation in the cytoplasm.

It has been reported that m-GluR I is expressed widely in retinal cells [28, 57–59]. We have previously demonstrated that RGCs mainly express the mGluR1 subtype, while Müller cells principally express the m-GluR5 subtype [28, 60]. Under physiological conditions, the endogenous release of glutamate from bipolar cells constantly modulates RGC firing by activating m-GluR I. The m-GluR I agonist, DHPG, increases RGC excitability and causes depolarization by inhibiting inwardly-rectifying K^+ channels (Kir) and hyperpolarization-activated cation channels [28]. Conditional knockout of Rac1 in RGCs significantly reduced m-GluR1 protein levels (Fig. 4), which may have decreased RGC excitability and resulted in hyperpolarization of the membrane potential. Whether the changes of m-GluR1 in Rac1-cKO mice modulates the synaptic transmission of RGCs remains to be explored. It is of interest that expression of the m-GluR5 subunit was increased due to conditional knockout of Rac1. Because this subunit is mainly expressed in Müller cells and is involved in Müller cell gliosis in rats with experimental glaucoma [60], its effect remains to be addressed in future studies.

Previous studies have shown that the small GTPases, including RhoA, Rac1, and Cdc42, are key regulators of cytoskeletal reorganization in dendrites and spines, and play important roles in dendritic spine morphology and plasticity [61–69]. Consistent with our results, the

expression of dominant-negative mutants of Rac1 cause a marked reduction in the number of primary dendrites in non-pyramidal neurons [42], while the expression of the constitutively active form of Rac1 to enhance Rac1 activity selectively increases dendritic branch additions and retractions in single optic tectal neurons of albino *Xenopus* tadpoles [70] and causes dendrite hyperproliferation in *Xenopus* RGCs [40]. In addition, abnormalities in dendrites and dendritic spines are associated with several psychiatric and neurological diseases. The effects of the small GTPases on dendrites could be mediated by modulating NMDARs. For example, inactivation of RhoA, but not Rac1 and Cdc42, in rat hippocampal neurons results in a rundown of somatodendritic NMDARs, which is mediated by its action on F-actin [65]. Overexpression of a non-kinase phorbol ester receptor, alpha1-chimerin, inhibits the formation of new spines and removes existing spines in cultured hippocampal neurons, and this is mediated by local inactivation of Rac1, indicating that a basal inhibition of Rac1 maintains the number of spines at a submaximal level. In addition, the effect of alpha1-chimerin is mediated by an interaction with the synaptic NR2A subunit of NMDARs [69]. In this study, we found that conditional knockout of Rac1 in RGCs increased the expression levels of the GluN1, GluN2A, and GluN2B subunits of NMDARs (Fig. 4), but did not change the dendritic spine-like branch density of RGCs. This phenomenon may be caused by conditional knockout of Rac1; meanwhile RhoA and Cdc42 may have compensated for the Rac1 deficiency-induced change in dendritic spine-like branches.

In the present study, we found an increased ratio of NMDA/AMPA EPSCs in the RGCs of Rac1-cKO mice. This may be a result of the changes in percentages of NMDA/AMPA receptors in each synapse although the total number of synapses was reduced, as evidenced by the decreased mEPSC frequency. It should be noted that a reduction of overall dendritic length would lead to a reduction of NMDA EPSCs. However, our results showed that the expression of NMDAR subunits in whole retinal extracts was slightly increased in Rac1-cKO mice (Fig. 4). The reasons for this discrepancy may be two-fold. The first is that the expression of functional NMDARs in RGCs may indeed be increased. In addition, the number of AMPARs in each synapse was not changed, as evidenced by the unchanged mEPSC amplitude. So, the ratio of NMDA/AMPA EPSCs was increased. However, it is inappropriate to compare the differences in NMDA and/or AMPA current amplitudes in different cells by recording eEPSCs because the intensity of stimulation and the location of stimulating electrodes were different. Furthermore, functional NMDARs are only expressed on the dendrites and dendritic spine-like branches in RGCs [71, 72], and we could not obtain dendritic samples to analyze the change in these receptors because of technical limitations. Another possible explanation is that Rac1 deletion may change the function of NMDARs in RGCs. Previous studies have reported that there is an interaction between Rac1 and NMDAR which affects spine morphogenesis and functions [2, 61, 73]. For example, in primary cultured neurons, inhibition of the activity of Rac1 and its main effector p21-activated kinase mediates the inhibitory effects of NMDARs containing GluN3 subunits on spine morphogenesis [61]. The Rac-specific GEF Tiam1 (T-lymphoma invasion and metastasis 1) seems likely to link NMDARs to affect spine development by activating particular Rac1-dependent signaling pathways that control actin cytoskeletal remodeling and protein synthesis [2]. Whether and how Rac1 deletion modulates the functions of dendritic NMDARs need to be characterized in future studies.

RGCs can be divided into many subtypes according to different classification criteria, mostly based on their physiological and morphological features [43, 74, 75]. In this study, the Lucifer Yellow-filled RGCs from control mice were morphologically classified according to the criteria of Sun *et al.* [43]. Our results showed that all five subtypes were present, and the percentage of RGCs in each subtype was similar to those of Sun *et al.* [43], suggesting that the RGCs used for our morphological analyses were randomly selected, and that potential bias was avoided. It should be noted that Rac1-cKO RGCs were not morphologically classified because the dendritic architecture of these cells may have been compromised [32].

In this study, the electrophysiological recordings were performed on RGCs in P17–P21 mice, while Western blot analysis was conducted using P70 mice. This raised the possibility that changes in mEPSCs/eEPSCs and GluA1 expression levels resulted from physiological development, and not from conditional knockout of Rac1. However, our results clearly showed that the GluA1 protein levels did not change during the postnatal period from 2W to 3M, demonstrating that it was the Rac1 deficiency that induced the changes of excitatory synaptic transmission in RGCs. In addition, we found that Rac1s were completely deleted at P17 (Fig. 1A), and the development of GluA1 protein in RGCs was completed by 2W (Fig. 6). These results suggest that the Rac1-cKO-induced changes in GluA1 expression in RGCs were finished before 2W. It is therefore reasonable to deduce that the changes in expression of both c-GluA1 and m-GluA1 occurred before 2W.

Unlike the excitatory synapses formed by dendritic spines, inhibitory synapses are formed directly by presynaptic terminals on dendritic membranes. It is notable that although conditional knockout of Rac1 reduced the dendritic complexity of RGCs, the inhibitory synaptic transmission was not affected, as evidenced by unchanged mIPSCs and glycine/$GABA_A$ receptor protein levels

(Figs. 2, 5). We speculate that conditional knockout of Rac1 may have induced dynamic structural reorganization of inhibitory synapses although mechanisms whose details remain to be explored.

Taken together, we have demonstrated that conditional deficiency of Rac1 in RGCs selectively attenuated excitatory synaptic transmission, which was mediated by reduced dendritic complexity and a reduced number of dendritic spine-like branches. In some retinal diseases, such as glaucoma, some subtypes of RGCs undergo significant changes in dendritic structure [76–78]. The selective activation of distinct Rac1-dependent pathways could improve survival and prevent dendrite degeneration of RGCs after optic nerve injury, suggesting that Rac1 may be a potential therapeutic target to counteract neuronal degenerative processes in the retina [15].

Acknowledgements This work was supported by grants from the National Natural Science Foundation of China (81790642, 31671078, and 81430007).

Conflict of interest The authors declare that the research was conducted in the absence of any commercial or financial relationships that could be construed as a potential conflict of interest.

References

1. Govek EE, Newey SE, Van Aelst L. The role of the Rho GTPases in neuronal development. Genes Dev 2005, 19: 1–49.
2. Tolias KF, Duman JG, Um K. Control of synapse development and plasticity by Rho GTPase regulatory proteins. Prog Neurobiol 2011, 94: 133–148.
3. Linseman DA, Loucks FA. Diverse roles of Rho family GTPases in neuronal development, survival, and death. Front Biosci 2008, 13: 657–676.
4. Ridley AJ. Rho GTPases and actin dynamics in membrane protrusions and vesicle trafficking Trends. Cell Biol 2006, 16: 522–529.
5. Hoffman GR, Nassar N, Cerione RA. Structure of the Rho family GTP-binding protein Cdc42 in complex with the multifunctional regulator RhoGDI. Cell 2000, 100: 345–356.
6. Zalcman G, Dorseuil O, Garcia-Ranea JA, Gacon G, Camonis J. RhoGAPs and RhoGDIs, (His)stories of two families. Prog Mol Subcell Biol 1999, 22: 85–113.
7. Bustelo XR, Sauzeau V, Berenjeno IM. GTP-binding proteins of the Rho/Rac family: regulation, effectors and functions *in vivo*. Bioessays 2007, 29: 356–370.
8. Cingolani LA, Goda Y. Actin in action: the interplay between the actin cytoskeleton and synaptic efficacy. Nat Rev Neurosci 2008, 9: 344–356.
9. Davis RL. Rac in the act of forgetting. Cell 2010, 140: 456–458.
10. Etienne-Manneville S, Hall A. Rho GTPases in cell biology. Nature 2012, 420: 629–635.
11. Hall A, Lalli G. Rho and Ras GTPases in axon growth, guidance, and branching. Cold Spring Harb Perspect Biol 2010, 2: a001818.
12. Shuai Y, Zhong Y. Forgetting and small G protein Rac Protein. Protein Cell 2010, 1: 503–506.
13. Mitchell DC, Bryan BA, Liu JP, Liu WB, Zhang L, Qu J, *et al.* Developmental expression of three small GTPases in the mouse eye. Mol Vis 2007, 13: 1144–1153.
14. Namekata K, Kimura A, Kawamura K, Guo X, Harada C, Tanaka K, *et al.* Dock3 attenuates neural cell death due to NMDA neurotoxicity and oxidative stress in a mouse model of normal tension glaucoma. Cell Death Differ 2013, 20: 1250–1256.
15. Lorenzetto E, Ettorre M, Pontelli V, Bolomini-Vittori M, Bolognin S, Zorzan S, *et al.* Rac1 selective activation improves retina ganglion cell survival and regeneration. PLoS One 2013, 8: e64350.
16. Dong N, Xu B, Shi H, Lu Y. miR-124 Regulates Amadori-Glycated Albumin-Induced Retinal Microglial Activation and Inflammation by Targeting Rac1. Invest Ophthalmol Vis Sci 2016, 57: 2522–2532.
17. Li YJ, Zhang J, Han J, Du ZJ, Wang P, Guo Y. Ras-related C3 botulinum toxin substrate 1 activation is involved in the pathogenesis of diabetic retinopathy. Exp Ther Med 2015, 9: 89–97.
18. Marc RE, Liu W. Fundamental GABAergic amacrine cell circuitries in the retina: nested feedback, concatenated inhibition, and axosomatic synapses. J Comp Neurol 2000, 425: 560–582.
19. Protti DA, Gerschenfeld HM, Llano I. GABAergic and glycinergic IPSCs in ganglion cells of rat retinal slices. J Neurosci 1997, 17: 6075–6085.
20. Wassle H. Parallel processing in the mammalian retina. Nat Rev Neurosci 2004, 5: 747–757.
21. Wassle H, Boycott BB. Functional architecture of the mammalian retina. Physiol Rev 1991, 71: 447–480.
22. Dong LD, Gao F, Wang XH, Miao Y, Wang SY, Wu Y, *et al.* GluA2 trafficking is involved in apoptosis of retinal ganglion cells induced by activation of EphB/EphrinB reverse signaling in a rat chronic ocular hypertension model. J Neurosci 2015, 35: 5409–5421.
23. Gao F, Li F, Miao Y, Xu LJ, Zhao Y, Li Q, *et al.* Involvement of the MEK-ERK/p38-CREB/c-fos signaling pathway in Kir channel inhibition-induced rat retinal Muller cell gliosis. Sci Rep 2017, 7: 1480.
24. Li C, Chen T. A novel hematoxylin and eosin stain assay for detection of the parasitic dinoflagellate amoebophrya. Harmful Algae 2017, 62: 30–36.
25. Miao Y, Dong LD, Chen J, Hu XC, Yang XL, Wang Z. Involvement of calpain/p35–p25/Cdk5/NMDAR signaling pathway in glutamate-induced neurotoxicity in cultured rat retinal neurons. PLoS One 2012, 7: e42318.
26. Cui P, Li XY, Zhao Y, Li Q, Gao F, Li LZ, *et al.* Activation of dopamine D1 receptors enhances the temporal summation and excitability of rat retinal ganglion cells. Neuroscience 2017, 355: 71–83.
27. Wang XH, Wu Y, Yang XF, Miao Y, Zhang CQ, Dong LD, *et al.* Cannabinoid CB1 receptor signaling dichotomously modulates inhibitory and excitatory synaptic transmission in rat inner retina. Brain Struct Funct 2016b, 221: 301–316.
28. Li Q, Cui P, Miao Y, Gao F, Li XY, Qian WJ, *et al.* Activation of group I metabotropic glutamate receptors regulates the excitability of rat retinal ganglion cells by suppressing Kir and I h. Brain Struct Funct 2017, 222: 813–830.
29. Qian WJ, Yin N, Gao F, Miao Y, Li Q, Li F, *et al.* Cannabinoid CB1 and CB2 receptors differentially modulate L- and T-type Ca^{2+} channels in rat retinal ganglion cells. Neuropharmacology 2017, 124: 143–156.
30. Ramoa AS, Campbell G, Shatz CJ. Dendritic growth and remodeling of cat retinal ganglion cells during fetal and postnatal development. J Neurosci 1988, 8: 4239–4261.

31. Liu HM, Sang SM, Lu Y, Wang ZF, Yu X, Zhong CJ. Thiamine metabolism is critical for regulating correlated growth of dendrite arbors and neuronal somata. Sci Rep 2017, 7: 5342.
32. Williams PA, Thirgood RA, Oliphant H, Frizzati A, Littlewood E, Votruba M, *et al.* Retinal ganglion cell dendritic degeneration in a mouse model of Alzheimer's disease. Neurobiol Aging 2013, 34: 1799–1806.
33. Zhao Y, Li Q, Li XY, Cui P, Gao F, Zhu K, *et al.* Involvement of mGluR I in EphB/ephrinB reverse signaling activation induced retinal ganglion cell apoptosis in a rat chronic hypertension model. Brain Res 2018, 1683: 27–35.
34. Erickson CS, Lee SJ, Barlow-Anacker AJ, Druckenbrod NR, Epstein ML, Gosain A. Appearance of cholinergic myenteric neurons during enteric nervous system development: comparison of different ChAT fluorescent mouse reporter lines. Neurogastroenterol Motil 2014, 26: 874–884.
35. Ivanova E, Hwang GS, Pan ZH. Characterization of transgenic mouse lines expressing Cre recombinase in the retina. Neuroscience 2010, 165: 233–243.
36. Bongmba OY, Martinez LA, Elhardt ME, Butler K, Tejada-Simon MV. Modulation of dendritic spines and synaptic function by Rac1: a possible link to Fragile X syndrome pathology. Brain Res 2011, 1399: 79–95.
37. Lee T, Winter C, Marticke SS, Lee A, Luo L. Essential roles of Drosophila RhoA in the regulation of neuroblast proliferation and dendritic but not axonal morphogenesis. Neuron 2000, 25: 307–316.
38. Luo L, Hensch TK, Ackerman L, Barbel S, Jan LY, Jan YN. Differential effects of the Rac GTPase on Purkinje cell axons and dendritic trunks and spines. Nature 1996, 379: 837–840.
39. Nakayama AY, Harms MB, Luo L. Small GTPases Rac and Rho in the maintenance of dendritic spines and branches in hippocampal pyramidal neurons. J Neurosci 2000, 20: 5329–5338.
40. Ruchhoeft ML, Ohnuma S, McNeill L, Holt CE, Harris WA. The neuronal architecture of Xenopus retinal ganglion cells is sculpted by rho-family GTPases in vivo. J Neurosci 1999, 19: 8454–8463.
41. Tashiro A, Minden A, Yuste R. Regulation of dendritic spine morphology by the Rho family of small GTPases: Antagonistic roles of Rac and Rho. Cereb Cortex 2000, 10: 927–938.
42. Threadgill R, Bobb K, Ghosh A. Regulation of dendritic growth and remodeling by Rho, Rac, and Cdc42. Neuron 1997, 19: 625–634.
43. Sun W, Li N, He S. Large-scale morphological survey of mouse retinal ganglion cells. J Comp Neurol 2002, 451: 115–126.
44. Caserta F, Eldred WD, Fernandez E, Hausman RE, Stanford LR, Bulderev SV, *et al.*. Determination of fractal dimension of physiologically characterized neurons in two and three dimensions. J Neurosci Methods 1995, 56: 133–144.
45. Duan H, Wearne SL, Rocher AB, Macedo A, Morrison JH, Hof PR. Age-related dendritic and spine changes in corticocortically projecting neurons in macaque monkeys. Cereb Cortex 2003, 13: 950–961.
46. Gutierrez H, Davies AM. A fast and accurate procedure for deriving the Sholl profile in quantitative studies of neuronal morphology. J Neurosci Methods 2007, 163: 24–30.
47. Haas K, Li J, Cline HT. AMPA receptors regulate experience-dependent dendritic arbor growth *in vivo*. Proc Natl Acad Sci U S A 2006, 103: 12127–12131.
48. Lowndes M, Stanford D, Stewart MG. A system for the reconstruction and analysis of dendritic fields. J Neurosci Methods 1990, 31: 235–245.
49. Robinson TE, Kolb B. Persistent structural modifications in nucleus accumbens and prefrontal cortex neurons produced by previous experience with amphetamine. J Neurosci 1997, 17: 8491–8497.
50. Zagrebelsky M, Holz A, Dechant G, Barde YA, Bonhoeffer T, Korte M. The p75 neurotrophin receptor negatively modulates dendrite complexity and spine density in hippocampal neurons. J Neurosci 2005, 25: 9989–9999.
51. Sholl DA. Dendritic organization in the neurons of the visual and motor cortices of the cat. J Anat 1953, 87: 387–406.
52. Branda CS, Dymecki SM. Talking about a revolution: The impact of site-specific recombinases on genetic analyses in mice. Dev Cell 2004, 6: 7–28.
53. Nagy A. Cre recombinase: the universal reagent for genome tailoring. Genesis 2000, 26: 99–109.
54. Larsen AK, Osborne NN. Involvement of adenosine in retinal ischemia. Studies on the rat. Invest Ophthalmol Vis Sci 1996, 37: 2603–2611.
55. Rom S, Fan S, Reichenbach N, Dykstra H, Ramirez SH, Persidsky Y. Glycogen synthase kinase 3beta inhibition prevents monocyte migration across brain endothelial cells via Rac1-GTPase suppression and down-regulation of active integrin conformation. Am J Pathol 2012, 181: 1414–1425.
56. Rom S, Zuluaga-Ramirez V, Dykstra H, Reichenbach NL, Pacher P, Persidsky Y. Selective activation of cannabinoid receptor 2 in leukocytes suppresses their engagement of the brain endothelium and protects the blood-brain barrier. Am J Pathol 2013, 183: 1548–1558.
57. Dyka FM, May CA, Enz R. Metabotropic glutamate receptors are differentially regulated under elevated intraocular pressure. J Neurochem 2004, 90: 190–202.
58. Koulen, P, Kuhn R, Wassle H, Brandstatter JH. Group I metabotropic glutamate receptors mGluR1alpha and mGluR5a: localization in both synaptic layers of the rat retina. J Neurosci 1997, 17: 2200–2211.
59. Tehrani A, Wheeler-Schilling TH, Guenther E. Coexpression patterns of mGLuR mRNAs in rat retinal ganglion cells: a single-cell RT-PCR study. Invest Ophthalmol Vis Sci 2000, 41: 314–319.
60. Ji M, Miao Y, Dong LD, Chen J, Mo XF, Jiang, SX, *et al.* Group I mGluR-mediated inhibition of Kir channels contributes to retinal Muller cell gliosis in a rat chronic ocular hypertension model. J Neurosci 2012, 32: 12744–12755.
61. Fiuza M, Gonzalez-Gonzalez I, Perez-Otano I. GluN3A expression restricts spine maturation *via* inhibition of GIT1/Rac1 signaling. Proc Natl Acad Sci U S A 2013, 110: 20807–20812.
62. Konstantoudaki X, Chalkiadaki K, Tivodar S, Karagogeos D, Sidiropoulou K. Impaired synaptic plasticity in the prefrontal cortex of mice with developmentally decreased number of interneurons. Neuroscience 2016, 322: 333–345.
63. Martinez LA, Tejada-Simon MV. Pharmacological inactivation of the small GTPase Rac1 impairs long-term plasticity in the mouse hippocampus. Neuropharmacology 2011, 61: 305–312.
64. Mi Z, Si T, Kapadia K, Li Q, Muma NA. Receptor-stimulated transamidation induces activation of Rac1 and Cdc42 and the regulation of dendritic spines. Neuropharmacology 2017, 117: 93–105.
65. Norenberg W, Hofmann F, Illes P, Aktories K, Meyer DK. Rundown of somatodendritic N-methyl-D-aspartate (NMDA) receptor channels in rat hippocampal neurones: evidence for a role of the small GTPase RhoA. Br J Pharmacol 1999, 127: 1060–1063.
66. Okabe T, Nakamura T, Nishimura YN, Kohu K, Ohwada S, Morishita Y, *et al*. RICS, a novel GTPase-activating protein for Cdc42 and Rac1, is involved in the beta-catenin-N-cadherin and N-methyl-D-aspartate receptor signaling. J Biol Chem 2003, 278: 9920–9927.
67. Schwechter B, Rosenmund C, Tolias KF. RasGRF2 Rac-GEF activity couples NMDA receptor calcium flux to enhanced

synaptic transmission. Proc. Natl. Acad. Sci. U S A 2013, 110: 14462–14467.
68. Sild M, Van Horn MR, Schohl A, Jia D, Ruthazer ES. Neural activity-dependent regulation of radial glial filopodial motility is mediated by glial cGMP-dependent protein kinase 1 and contributes to synapse maturation in the developing visual system. J Neurosci 2016, 36: 5279–5288.
69. Van de Ven TJ, VanDongen HM, VanDongen AM. The nonkinase phorbol ester receptor alpha 1-chimerin binds the NMDA receptor NR2A subunit and regulates dendritic spine density. J Neurosci 2005, 25: 9488–9496.
70. Li Z, Van Aelst L, Cline HT. Rho GTPases regulate distinct aspects of dendritic arbor growth in Xenopus central neurons *in vivo*. Nat Neurosci 2000, 3: 217–225.
71. Zhang J, Diamond JS. Distinct perisynaptic and synaptic localization of NMDA and AMPA receptors on ganglion cells in rat retina. J Comp Neurol 2006, 498: 810–820.
72. Zhang J, Diamond JS. Subunit- and pathway-specific localization of NMDA receptors and scaffolding proteins at ganglion cell synapses in rat retina. J Neurosci 2009, 29: 4274–4286.
73. Xiao L, Hu C, Yang W, Guo D, Li C, Shen W, *et al.* NMDA receptor couples Rac1-GEF Tiam1 to direct oligodendrocyte precursor cell migration. Glia 2013, 61: 2078–2099.
74. Doi M, Uji Y, Yamamura, H. Morphological classification of retinal ganglion cells in mice. J Comp Neurol 1995, 356: 368–386.
75. Wang J, Jacoby R, Wu SM. Physiological and morphological characterization of ganglion cells in the salamander retina. Vis Res 2016a, 119: 60–72.
76. El-Danaf RN, Huberman AD. Characteristic patterns of dendritic remodeling in early-stage glaucoma: evidence from genetically identified retinal ganglion cell types. J Neurosci 2015, 35: 2329–2343.
77. Della Santina L, Inman DM, Lupien CB, Horner PJ, Wong RO. Differential progression of structural and functional alterations in distinct retinal ganglion cell types in a mouse model of glaucoma. J Neurosci 2013, 33:17444–17457.
78. Yang LC, Ren P, Ma YY. Anodal transcranial direct-current stimulation over the right dorsolateral prefrontal cortex influences emotional face perception. Neurosci Bull 2018, 34: 842–848.